PAPER

Check for updates

In situ ATR-FTIR investigation and theoretical calculation of the interactions of chromate and citrate on the surface of haematite (α-Fe$_2$O$_3$)

W. G. Gao, [iD]^{ac} X. C. Liu^b and M. F. Chen*^{a}

In situ attenuated total reflectance Fourier transform infrared (ATR-FTIR) spectroscopy was used to study the molecular kinetics of Cr(VI) reduction by citric acid at the α-Fe$_2$O$_3$–water interface. Both citrate and Cr(VI) were adsorbed to the surface of α-Fe$_2$O$_3$ through the formation of stable monodentate and bidentate complexes. Chromate was potentially reduced by citric acid hydroxyl groups (−COO$^-$) on the α-Fe$_2$O$_3$ surface sites. Monodentate complexes were favoured at pH 4.0 due to strong electrostatic attraction forces between the ions and minerals. Density functional theory was used to calculate the adsorption and interaction processes of Cr(VI) and citrate on α-Fe$_2$O$_3$; the calculations indicated that the adsorption of Cr(VI) or citrate can occur spontaneously and result in the formation of stable complexation structures. However, the co-adsorption of Cr(VI) and citrate on α-Fe$_2$O$_3$ is energetically unstable and leads to the initiation of redox reactions on the α-Fe$_2$O$_3$ surface. These findings have important implications for the fate of chromate in the environment. Therefore, our work describes the molecular mechanism of Cr(VI) reduction by citrate on the surface of α-Fe$_2$O$_3$ for the first time. The results can be correlated to the fate of chromate in the environment in the presence of α-Fe$_2$O$_3$ and low molecular weight organic acids.

1 Introduction

Chromium(VI) (Cr(VI)) is one of the most frequently detected industrial groundwater contaminants. Cr(VI) is a carcinogen, and it exists in an oxyanionic form as chromate. The fate of Cr(VI) depends on its adsorption reactions on mineral surfaces in the absence of reducing conditions.[1] Adsorption onto minerals is a common method for removing Cr(VI) from the environment.[2] The reduction of Cr(VI) to Cr(III) is another important strategy for detoxifying Cr(VI)-contaminated sites, and it is an effective treatment method.

Several studies have investigated the rapid removal of Cr(VI) from solutions using different types of adsorbents, such as metal oxides,[3] and minerals.[4] The molecular mechanisms of Cr(VI) adsorption on iron oxides were recently investigated by Johnston *et al.*,[5] who used theoretical calculations and *in situ* attenuated total reflected Fourier transformed infrared spectroscopy (ATR-FTIR) to elucidate the adsorption structure of Cr(VI) on the surface of hematite. Cr(VI) can also be reduced to Cr(III) using natural organic matter (NOM); this process is

greatly affected by the presence of coexisting metal ions[6] and the properties of the minerals.[7]

The interactions between Cr(VI) and natural organic acids at mineral–water interfaces have become an increasingly important area of interest when considering the behaviour and toxicity of Cr(VI) in the environment. As one of the most ubiquitous natural organic acids, citric acid is an exudate of plants and can reduce Cr(VI) into Cr(III) under certain conditions. Earlier studies have confirmed that mineral surfaces can act as catalysts for redox reactions between Cr(VI) and citric acids to form nontoxic Cr(III).[8–11] But the molecular mechanisms of their interactions at mineral–water interfaces remain unclear.

In this study, the molecular kinetics of Cr(VI) reduction by citrate on the surface of α-Fe$_2$O$_3$ was investigated *in situ* by using ATR-FTIR spectroscopy. Density functional theory (DFT) was used to calculate the electron densities and variations of the interactions between Cr(VI) and citrate at Fe$_2$O$_3$–water interfaces with different environmentally relevant pH values. We hypothesized that negatively charged Cr(VI) and citrate would adsorb to the positively charged α-Fe$_2$O$_3$ surface through the formation of monodentate complexes due to electrostatic attraction. Based on this assumption, the binding and free energies of the clusters were calculated to infer their possible reaction pathways. Our findings elucidate how these reactions occur at the molecular level.

^{a}Key Laboratory of Soil Environment and Pollution Remediation, Institute of Soil Science, Chinese Academy of Sciences, Nanjing 210008, China. E-mail: mfchen@issas.ac.cn

^{b}State Key Laboratory for Coal Conversion, Institute of Coal Chemistry, Chinese Academy of Sciences, Taiyuan 130100, China

^{c}University of the Chinese Academy of Sciences, Beijing 100049, China

2 Materials and methods

2.1 Chemicals

All chemicals and reagents were of analytical grade or higher purity and were used as received, and all solutions were prepared using Millipore filtered water (18 MΩ, Millipore Corp.). α-Fe_2O_3 was purchased from Sino Chemicals Corp., with a purity of more than 99.9%. Powder X-ray diffraction (XRD) was used to determine the bulk crystalline phase of the α-Fe_2O_3. The BET surface area of the studied α-Fe_2O_3 was 4.08 ± 0.02 $m^2\ g^{-1}$. For *in situ* ATR-FTIR experiments, α-Fe_2O_3 was suspended in Millipore water by sonicating for 6 hours before use.

## 2.2 *In situ* ATR-FTIR analysis

In situ flow cell ATR-FTIR spectroscopy was performed using a Bruker FTIR (Bruker Optics) spectrometer equipped with a multi-bounce PIKE flow cell part (PIKE Corp.). Data collection and analyses were performed using the OPUS software package (v6.5). Scans were recorded from 4000 to 400 cm^{-1} at a resolution of 8 cm^{-1}. α-Fe_2O_3 film coatings (~0.5 mg) were prepared by depositing 0.8 mL of the α-Fe_2O_3 suspension on a ZnSe internal reflection element (IRE) and were dried under a stream of nitrogen gas. Next, the IRE was mounted on a flow cell with a peristaltic pump to allow a specified volume of solution to pass over the film. The concentrations of Cr(vi) and citric acid were set at 0.1 mM each, and the solution pH was adjusted by titrating with 0.1 M HNO_3 or NaOH. Before the adsorption experiment, the film was equilibrated with H_2O (18 MΩ) at the specified pH for 20 min. The flow rate was set to approximately 1 mL min^{-1}.

2.3 DFT calculations

The theoretical frequencies of the possible surface complex structures were calculated using the approach described by Kubicki *et al.*[12] The Fe_2O_3 surface was represented using an $Fe_2O_xH_y$ di-iron hydroxide cluster model that consisted of two octahedrally coordinated Fe atoms connected *via* two Fe–(OH)–Fe linkages. This model has been used in many other theoretical studies and has been proven valid. All calculations were performed using the Gaussian09 package and run on the Tianhe-2 supercomputer at the LvLiang Cloud Computing Center. DFT calculations were performed using the B3LYP method[5,13] and the 6-311G++(d,p) basis set. The geometries of the clusters were optimized using the Berny algorithm and GEDIIS with redundant internal coordinates to a potential energy minimum without symmetry or geometrical constraints. Next, the clusters were analysed for harmonic frequencies. Short-range solvation effects were accounted for by using 3 explicit water molecules, and the long-range solvation effect was modelled using the integral equation formalism version of the polarizable continuum model (PCM).[14] All atomic charges were calculated based on the natural bond orbital (NBO) population analysis code in Gaussian09.

Because the Fe_2O_3 surface should be protonated and saturated with water molecules in aqueous solutions, the adsorption of either $HCrO_4^-$ or citrate would not occur unless one or more of the saturating H_2O molecules were replaced by the adsorbents. We defined the adsorption energy and free energy by using the following chemical equation:

$$\text{Ion} + \text{cluster} \cdot 3H_2O = \text{ion\_cluster} \cdot 4H_2O \tag{1}$$
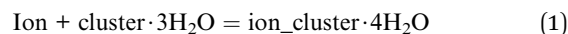
where "ion_cluster·$4H_2O$" indicates the substitution of a coordinating water molecule with an incoming ion and the water molecule becomes an additional explicit solvent molecule.

Thus we have:

$$\Delta E_{ad} = E(\text{ion\_cluster} \cdot 4H_2O) - E(\text{ion}) - E(\text{cluster} \cdot 3H_2O) \tag{2}$$

$$\Delta G_{ad} = G(\text{ion\_cluster} \cdot 4H_2O) - G(\text{ion}) - G(\text{cluster} \cdot 3H_2O) \tag{3}$$

In the case of co-adsorption,

$$\Delta E_{ad} = E(\text{ionA\_ionB\_cluster} \cdot 5H_2O) - E(\text{ionA}) - E(\text{ionB}) \\ - E(\text{cluster} \cdot 3H_2O) \tag{4}$$

$$\Delta G_{ad} = G(\text{ionA\_ionB\_cluster} \cdot 5H_2O) - G(\text{ionA}) - G(\text{ionB}) \\ - G(\text{cluster} \cdot 3H_2O) \tag{5}$$

3 Results and discussion

3.1 *In situ* ATR-FTIR studies of Cr(vi) and citrate on α-Fe_2O_3

3.1.1 Adsorption of Cr(vi) on the Fe_2O_3 film as a function of time and pH. Fig. 1 displays the ATR-FTIR spectra of α-Fe_2O_3 exposed to 0.1 mM chromate at pH 2.0, 4.0, 6.0 and 8.0 (as shown in Fig. 1A, B, C and D, respectively) as a function of time. The depicted frequency range corresponding to the region of Cr–O stretching vibrations of $HCrO_4^-$ and CrO_4^{2-} in solution is between 800 and 950 cm^{-1}.[15] The chromate signals in Fig. 1
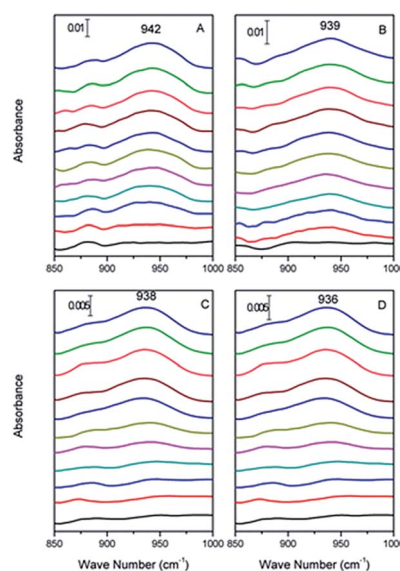

Fig. 1 *In situ* ATR-FTIR spectrum of Cr(vi) adsorbed on haematite film at pH (A) 2.0, (B) 4.0, (C) 6.0, and (D) 8.0, respectively, from 0 to 30 min (from bottom to top).
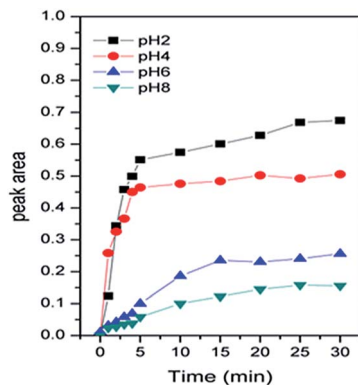
Fig. 2 Areas of the IR peaks from Cr(VI) adsorbed on haematite at different pH values.

Fig. 4 Areas of the IR peaks from the carboxyl radicals (−COO⁻) of citrate adsorbed on haematite at different pH values.

were attributed to its adsorption on the α-Fe$_2$O$_3$ because the chromate concentration in solution (0.1 mM) was well below the detection limit (>10 mM).

Specifically, the Cr(VI) adsorbed on α-Fe$_2$O$_3$ resulted in spectral features at 942, 939, 938 and 936 cm^{-1} at pH 2.0, 4.0, 6.0, and 8.0, respectively. In addition, the data obtained for pH 2.0, 4.0, 6.0 and 8.0 showed similar vibrational modes of Cr–O that increased with time and reached equilibrium after 30 min with no visible changes. We attributed the increased intensity of the spectral features representing associated Cr(VI) to its adsorption to the α-Fe$_2$O$_3$ surface. To qualify the interface absorption kinetics of Cr(VI), the peak areas of the Cr–O stretching vibrations at each specific pH were calculated as a function of time, as shown in Fig. 2, which is consistent with the expectation that chromate absorption on the α-Fe$_2$O$_3$ increased as the pH decreased, as previously overserved in batch studies.[16,17]

3.1.2 Adsorption of citric acid on the Fe$_2$O$_3$ film as a function of time and pH. Fig. 3 displays the ATR-FTIR spectra of citric acid adsorbed on α-Fe$_2$O$_3$ film at pH 2.0, 4.0, 6.0 and 8.0 (Fig. 3A,

B, C and D, respectively) as a function of time. Similar to Cr(VI) adsorption, spectral features resulted from the sorption of citric acid to the α-Fe$_2$O$_3$ film. The most representative citric acid radicals were –COOH and –COO⁻, and protons were hydrolysed from the citric acid molecules. The carbonyl double bond ($v_{C=O}$) of the –COOH radical resulted in a peak at 1740 cm^{-1}, the single carboxyl radical resulted in a peak at 1740 cm^{-1}, and the single carboxyl bond ($v_{C–OH}$) position of the –COOH radical resulted in a peak at 1270 cm^{-1}, as reported by Bhandari et al.[18] and Max and Chapados.[19] The peak at 1400 cm^{-1} was interpreted as the symmetric vibrations of ionized –COO⁻ radicals ($v_s(COO^-)$), and the frequency range of 1570–1595 cm^{-1} was attributed to the asymmetric vibrations of the ionized –COO⁻ radicals ($v_{as}(COO^-)$).[19] The intensity of the peaks from the vibrations of these radicals slightly changed with pH, especially the intensities of $v_{as}(COO^-)$ and $v_s(COO^-)$ as the hydrolysis of protons from the citric acid occurred with increasing pH.

Within the equilibrium pH range, citric acids were expected to gradually dissociate and remain deprotonated (negatively charged), and the surface of α-Fe$_2$O$_3$ was expected to remain positively charged (pH$_{zeta}$ $\approx$ 8.4). The –COO⁻ radicals become adsorbed to the α-Fe$_2$O$_3$ surface via electrostatic attraction when the solution pH is greater than the pK_{a1} of citric acid. The areas of the $v_{as}(COO^-)$ and $v_s(COO^-)$ peaks were calculated to study their absorption kinetics on the α-Fe$_2$O$_3$ surface, as shown in Fig. 4A and B, respectively. As the pH increased, the intensities of $v_{as}(COO^-)$ and $v_s(COO^-)$ increased and were maximized at pH 6.0. Although the maximum electronegativity of citric acid should occur at pH > 8.0, the surface of α-Fe$_2$O$_3$ is negatively charged when the solution pH is greater than its isoelectric point, which would prevent the adsorption of more –COO⁻ radicals on α-Fe$_2$O$_3$.

3.1.3 Sequent exposure of Cr(VI) and citrate. Fig. 5 displays the in situ ATR-FTIR results of the sequential flow of 0.1 mM Cr(VI) and 0.1 mM citric acid solutions at pH 4.0 on α-Fe$_2$O$_3$ film (A and B, respectively) as a function of time. The ATR-absorbance signal of bichromate on the α-Fe$_2$O$_3$ film increased with time in our experiment (Fig. 5A(a, b, c, d and e), respectively) and exhibited a characteristic spectral peak at 942 cm^{-1}. The increased intensity of the Cr(VI) at this stage was attributed to its adsorption on the α-Fe$_2$O$_3$ film. The intensity of
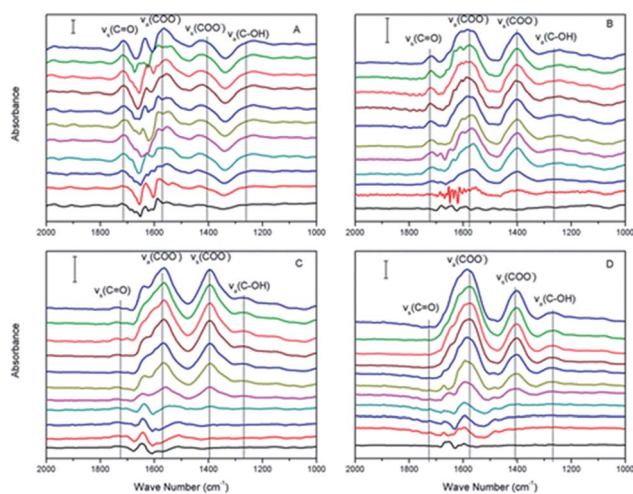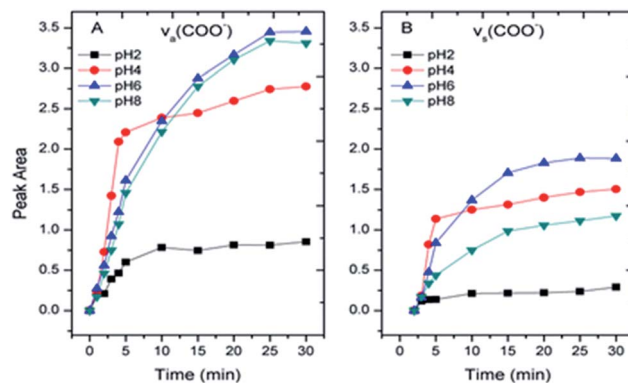

Fig. 3 In situ ATR-FTIR spectra of citrate adsorbed on haematite film at pH (A) 2.0, (B) 4.0, (C) 6.0, and (D) 8.0, respectively, from 0 to 30 min (from bottom to top).
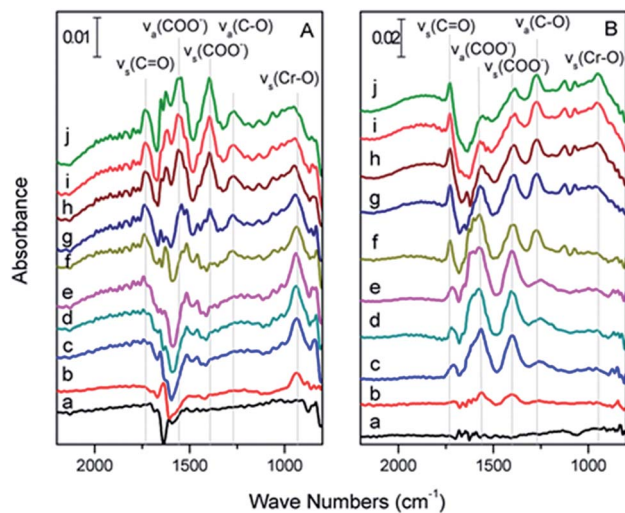
Fig. 5 (A) *In situ* ATR-FTIR spectrum of haematite (a) flushed with pH 4.0 H_2O for 15 min and after subsequent exposure to a flowing solution of 0.1 mM Cr(VI) at pH 4.0 for (b) 1, (c) 5, (d) 15 and (e) 30 min and (f) flushed with pH 4 H_2O for 20 min and after subsequent exposure to a flowing solution of 0.1 mM citric acid at pH 4 for (g) 1, (h) 5, (i) 15, and (j) 30 min (B) *in situ* ATR-FTIR spectrum of haematite (a) flushed with pH 4.0 H_2O for 15 min and after subsequent exposure to a flowing solution of 0.1 mM citric acid at pH 4.0 for (b) 1, (c) 5, (d) 15 and (e) 30 min; and (f) flushed with pH 4 H_2O for 20 min and after subsequent exposure to a flowing solution of Cr(VI) 0.1 mM at pH 4 for (g) 1, (h) 5, (i) 15, and (j) 30 min.

ν(Cr=O) slightly decreased after flushing with water at pH 4 for 20 min until equilibrium was reached (Fig. 5A-f), at which time 0.1 mM citric acid at pH 4 was introduced into the ATR flow cell. The intensity of ν(Cr=O) gradually decreased and disappeared after 30 min. However, this result did not exclude the adsorbed Cr(VI) that was displaced by the citric acid *via* a competitive adsorption mechanism.

During the flow sequence, the characteristic peaks of citric acid grew with time (Fig. 5B(a, b, c, d, and e), respectively), which meant that the citric acid was adsorbed on the α-Fe$_2$O$_3$ film. Because –COOH and –COO$^-$ had different vibration modes, as mentioned above, we inferred that the –COOH and –COO$^-$ functional groups of citric acid were both adsorbed to the α-Fe$_2$O$_3$ surface. The vibration intensity of the citric acid remained stable when flushed with water at pH 4 water (Fig. 5B-f) for 20 min, at which time the pH 4.0 Cr(VI) solution was pumped into the ATR flow cell. Interestingly, as the intensity of the ν(Cr=O) peak increased, the intensities of the ν_s(COO$^-$) and ν_{as}(COO$^-$) peaks gradually decreased. However, the intensities of the ν_s(C=O) and ν_{as}(C–O) peaks of the –COOH radicals remained the same throughout the experiment (Fig. 5B(g, h, i and j), respectively), which indicated that the adsorbed –COO$^-$ radical was the electron supplier rather than the –COOH radical of citric acid.

3.2 DFT calculations

3.2.1 The structures and adsorption energetics of citrate and Cr(VI) on Fe$_2$O$_3$. The optimized structures of the di-iron
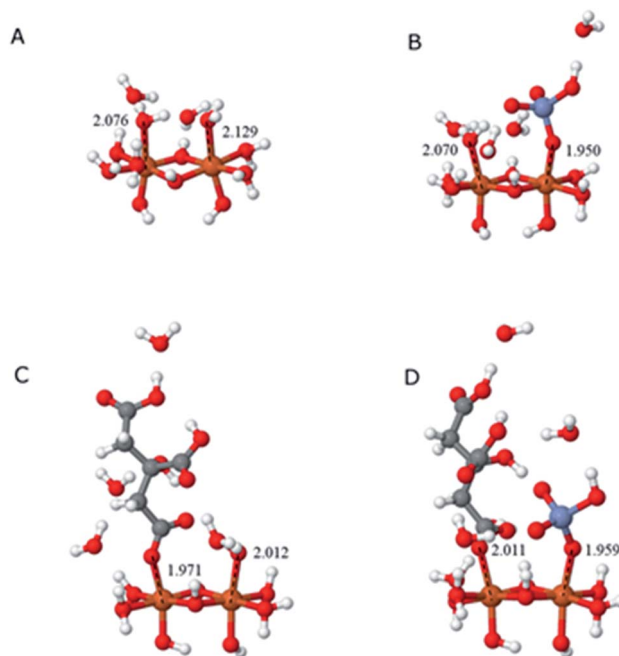

Fig. 6 The optimized structures of the di-iron hydroxide cluster (A), with HCrO$_4^-$ adsorption (B), citrate adsorption (C), and HCrO$_4^-$ and citrate co-adsorption (D). Fe: orange, O: red, Cr: dark blue, C: grey, and H: white.

clusters and their adsorbed species are shown in Fig. 6. In the di-iron cluster, the water molecules were loosely coordinated with the Fe atoms. The adsorption of citrate and HCrO$_4^-$ ions decreased the Fe–O distance, which indicted that both ions were more strongly bound to the Fe–O bonds. This result was confirmed by the negative adsorption energy changes shown in Table 1. Both citrate and HCrO$_4^-$ ions have similar adsorption energies of approximately −70 kJ mol^{-1}.

The co-adsorption state (−106.25 kJ mol^{-1}) is energetically less favourable than the independent adsorption of both ions (153.05 kJ mol^{-1}), presumably due to steric electronic effects.

As expected, adsorption causes monomers to lose some degree of freedom and is unfavourable in terms of entropy change. This effect is reflected by the difference in the adsorption energies and the adsorption free energies. The entropic effect results in a co-adsorption free energy of only −1.38 kJ mol^{-1}; thus, the co-adsorption state is not very stable and may cause conformational changes, such as desorption or redox reactions. Redox reactions were favoured in this study.

3.2.2 The highest molecular orbitals (HOMO) and lowest unoccupied orbitals (LUMO) before and after citrate and Cr(VI) adsorption. The tendency of electron flow can be illustrated by the HOMO orbitals before and after adsorption. When considering an isolated citrate ion (Fig. 7C), the most active electrons (those in the HOMO orbital) mainly reside in carboxylate groups, which are negatively charged. When the carboxylate groups are adsorbed on the cluster, the most active electrons would move to the iron cluster (Fig. 7D). When HCrO$_4^-$ is further co-adsorbed (Fig. 7E), the most active electrons are shared by HCrO$_4^-$ and the iron cluster. In other words, some of

Table 1 Adsorption energy and free energy of the interactions of $HCrO_4^-$ and citrate with the di-iron hydroxide cluster

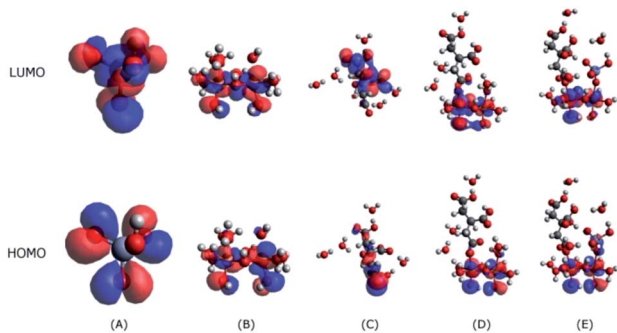| Energy	$HCrO_4^-$	Citrate	$HCrO_4^-$ + citrate
ΔE_{ad} (kJ mol^{-1})	−73.06	−79.99	−106.25
ΔG_{ad} (kJ mol^{-1})	−24.94	−38.51	−1.38

Fig. 7 The HOMO and LUMO levels of $HCrO_4^-$ (A), the Fe_2O_3 cluster (B), citrate (C), the citrate adsorption on the di-iron hydroxide cluster (D), and the citrate and $HCrO_4^-$ co-adsorption on the di-iron hydroxide cluster (E).

the active electrons flow from the iron cluster to $HCrO_4^-$. This result supports our hypothesis that Fe_2O_3 works as a bridge for the transfer of electrons between citrate and Cr(vi).

The interactions between citrate and Fe_2O_3 clusters involve electron flow from citrate to Fe_2O_3; hence, the HOMO orbitals of citrate will interact with the LUMO orbitals of Fe_2O_3 (Fig. 7B). As Fig. 7C shows, the HOMO orbital of citrate mostly resides on the bottom (carboxyl group), indicating that it will bind with Fe_2O_3 clusters through the carboxyl groups; this binding is evidenced by the interaction model in Fig. 7D. Despite the citrate adsorption, the LUMO orbital of the citrate–Fe_2O_3 complex is still located on the Fe_2O_3 part, showing that it still has the ability to attract $HCrO_4^-$ through the interaction between its LUMO orbital and the HOMO orbital of $HCrO_4^-$ (Fig. 7A). This observation proves that Fe_2O_3 is able to serve as a catalytic substrate for the co-adsorption and further reaction of citrate and $HCrO_4^-$, and this behaviour is in line with our experimental observations.

3.3 Reaction mechanisms

3.3.1 Adsorption mechanisms.
In situ ATR-FTIR spectroscopy showed that both Cr(vi) and citrate could adsorb to the α-Fe_2O_3 surface. Citric acid and chromate could be adsorbed on the α-Fe_2O_3 surface through electrostatic reactions, surface hydroxyl exchange or hydrogen bonding, which would result in absorbance IR spectra after the exposure of the solute to the α-Fe_2O_3 film.[20] The changes of the IR spectrum of the adsorbed chromate and citrate species on the α-Fe_2O_3 film can be considered to determine the number of structurally different surface complexes when considering their binding mode based on the absence or emergence of absorption bands and shifts in their frequency.

Johnston *et al.*[5] indicated chromate mainly formed inner sphere complexes with α-Fe_2O_3. From a quantitative point of view, the absorbance signal of the adsorbed chromate increased as the solution pH decreased in previous large batch studies.[21–25] Additionally, the spectra of adsorbed chromate on the α-Fe_2O_3 film were significantly different from the spectrum of aqueous chromate, which produced a single peak at 880 cm^{-1}.[26] Chromate is adsorbed to the α-Fe_2O_3 by electrostatic attraction and ligand exchange, resulting in the formation of monodentate complexes, with simultaneous desorption of surface hydroxyl groups from the iron surface sites. The complex geometry of the surface includes bidentate and monodentate complexes at low pH. Monodentate complexation is also a precursor for the formation of bidentate complexes.[27]

Citric acid can also adsorb onto α-Fe_2O_3 through electrostatic attraction and surface ligand exchange mechanisms.[28] Citric acid formed innersphere complexes with the surface of α-Fe_2O_3 (ref. 29) and symmetrical monodentate and bidentate surface complexes.[30] Protons generally dissociate from citric acid at three different pH values (pK_{a1} = 3.13, pK_{a2} = 4.76, and pK_{a3} = 6.40).[29] As shown in Fig. 3, the first two prominent IR bands were assigned to the asymmetric (ν_{as}) and symmetric (ν_s) stretching vibrations of the carboxylate (–COO$^-$) groups, which were located at 1570–1595 cm^{-1} and 1400 cm^{-1},[29] respectively. The bands at 1270 cm^{-1} and 1740 cm^{-1} were interpreted as the bands of vibrational stretching and bending of C=O and C–O in the –COOH groups of citric acid, respectively, because at least one carboxylic group likely remained in the protonated state under the experimental conditions (pH < pK_{a3}).[29] When the solution pH was greater than the pK_{a3}, these two bands gradually disappeared, as shown in Fig. 3. Therefore, citric acid could form monodentate or bidentate ring complexes with the α-Fe_2O_3 surface.[30]

3.3.2 Roles of α-Fe_2O_3 in electron and energy transport.
Several studies have suggested that small band gap semiconductors, such as ferrihydrite, goethite, TiO_2 and bayerite, can act as conduits for electron transfer between electron donors and acceptors.[8,31–33] The surface of α-Fe_2O_3 could also provide a pathway for energy and electron transport from the adsorbed citric acid to chromate. Batch experiments have confirmed that Cr(vi) could be reduced to Cr(iii) by citric acid in the presence of α-Fe_2O_3. According to the studies of Lan *et al.*[6,34] and Sarkar *et al.*,[7] however, citric acid could hardly reduce Cr(vi) in solution in the absence of minerals or metal ions.

The binding energies of different complexing structures of $HCrO_4^-$ and citric acid adsorbed on α-Fe_2O_3 at pH 4.0 were calculated by using DFT, as shown in Table 1. Both citrate and $HCrO_4^-$ ions have similar adsorption energies of approximately −70 kJ mol^{-1}. Co-adsorption could spontaneously occur because the free energy dropped significantly (−106.25 kJ mol^{-1}); however, the binding energy of the co-adsorption state remained relatively unchanged, which indicated that co-adsorption only occurred as a transitional state and was unstable. Based on calculations of the HOMO, the most active electron in citrate is concentrated in the –COO$^-$ radicals. The active electron density shifted to the Fe–O bond after citrate was adsorbed to an iron cluster. After co-adsorption with Cr(vi), the most active electrons

were shared by $HCrO_4^-$ and the iron cluster, indicating that electrons were transferred from the carboxyl groups of citrate to Cr(VI) via the Fe–O bond of α-Fe_2O_3.

4 Conclusions

This study provides molecular level insights regarding co-adsorption and the interactions of Cr(VI) and citrate on the α-Fe_2O_3 surface. The in situ ATR-FTIR spectroscopy results show that Cr(VI) and citrate adsorbed to the α-Fe_2O_3 surface and formed inner-sphere complexes. Furthermore, the DFT calculations indicated that the adsorption of both Cr(VI) and citrate on the surface of α-Fe_2O_3 was energetically favourable. The co-adsorption of ions on the surface of α-Fe_2O_3 could lead to electron transfer from the carboxyl group of citrate to Cr(VI), which would drive the reduction of Cr(VI) to Cr(III). Collectively, the in situ ATR-FTIR spectroscopy and adsorption energy results and the IR spectrum predicted by DFT theory show that the interactions between Cr(VI) and citrate at the α-Fe_2O_3–water interface can be theoretically and experimentally explained. Given the ubiquitous co-existence of α-Fe_2O_3 and low molecular weight organic acids in natural environments, this study could be used to understand the fundamental mechanisms that determine the fate of Cr(VI) in the environment.

Conflicts of interest

There are no conflicts of interest to declare.

Acknowledgements

References

1 C. P. Johnston and M. Chrysochoou, Environ. Sci. Technol., 2016, **50**, 3589–3596.

2 Z.-N. Huang, X.-L. Wang and D.-S. Yang, Water Sci. Eng., 2015, **8**, 226–232.

3 J. Hu, G. Chen and I. M. Lo, Water Res., 2005, **39**, 4528–4536.

4 K. Matern and T. Mansfeldt, Environ. Chem., 2016, **13**, 674–681.

5 C. P. Johnston and M. Chrysochoou, Geochim. Cosmochim. Acta, 2014, **138**, 146–157.

6 C. Li, Y.-Q. Lan and B.-L. Deng, Pedosphere, 2007, **17**, 318–323.

7 B. Sarkar, R. Naidu, G. S. R. Krishnamurti and M. Megharaj, Environ. Sci. Technol., 2013, **47**, 13629–13636.

8 B. Deng and A. T. Stone, Environ. Sci. Technol., 1996, **30**, 2484–2494.

9 J. W. Yang, Z. S. Tang, R. F. Guo and S. Q. Chen, Environ. Prog. Sustainable Energy, 2008, **27**, 302–307.

10 G. Yang, L. Tang, Y. Cai, G. Zeng, P. Guo, G. Chen, Y. Zhou, J. Tang, J. Chen and W. Xiong, RSC Adv., 2014, **4**, 58362–58371.

11 R. Dai, C. Yu, J. Liu, Y. Lan and B. Deng, Environ. Sci. Technol., 2010, **44**, 6959–6964.

12 J. D. Kubicki, K. D. Kwon, K. W. Paul and D. L. Sparks, Eur. J. Soil Sci., 2007, **58**, 932–944.

13 C. P. Johnston and M. Chrysochoou, Environ. Sci. Technol., 2012, **46**, 5851–5858.

14 E. Cancès, B. Mennucci and J. Tomasi, J. Chem. Phys., 1997, **107**, 3032.

15 K. Nakamoto, Infrared and Raman Spectra of Inorganic and Coordination Compounds, Theory and Applications in Inorganic Chemistry, Wiley, Hoboken, NJ, 2008.

16 V. T. Bodunde, F. A. Adekola and N. Abdus-Salam, J. N. C. Acad. Sci., 2013, **129**, 24–33.

17 S. Yin and D. E. Ellis, Surf. Sci., 2009, **603**, 736–746.

18 N. Bhandari, D. B. Hausner, J. D. Kubicki and D. R. Strongin, Langmuir, 2010, **26**, 16246–16253.

19 J.-J. Max and C. Chapados, J. Phys. Chem. A, 2004, **108**, 3324–3337.

20 K. Axe and P. Persson, Geochim. Cosmochim. Acta, 2001, **65**, 4481–4492.

21 D. Rai, L. Eary and J. Zachara, Sci. Total Environ., 1989, **86**, 15–23.

22 O. Ajouyed, C. Hurel, M. Ammari, L. B. Allal and N. Marmier, J. Hazard. Mater., 2010, **174**, 616–622.

23 D. D. Maksin, A. B. Nastasović, A. D. Milutinović-Nikolić, L. T. Suručić, Z. P. Sandić, R. V. Hercigonja and A. E. Onjia, J. Hazard. Mater., 2012, **209**, 99–110.

24 T. J. Reich and C. M. Koretsky, Geochim. Cosmochim. Acta, 2011, **75**, 7006–7017.

25 G. Du, Z. Li, L. Liao, R. Hanson, S. Leick, N. Hoeppner and W.-T. Jiang, J. Hazard. Mater., 2012, **221**, 118–123.

26 M. M. Hoffmann, J. G. Darab and J. L. Fulton, J. Phys. Chem. A, 2001, **105**, 1772–1782.

27 P. R. Grossl, M. Eick, D. L. Sparks, S. Goldberg and C. C. Ainsworth, Environ. Sci. Technol., 1997, **31**, 321–326.

28 W. Stumm and E. Wieland, in Aquatic Chemical Kinetics: Reaction Rates of Processes in Natural Waters. Environmental Science and Technology Series, ed. W. Stumm, John Wiley & Sons, New York, 1990, pp. 367–400.

29 I. A. Mudunkotuwa and V. H. Grassian, J. Am. Chem. Soc., 2010, **132**, 14986–14994.

30 O. W. Duckworth and S. T. Martin, Geochim. Cosmochim. Acta, 2001, **65**, 4289–4301.

31 D. E. Latta, J. E. Bachman and M. M. Scherer, Environ. Sci. Technol., 2012, **46**, 10614–10623.

32 B. Deng and A. T. Stone, Environ. Sci. Technol., 1996, **30**, 463–472.

33 B. Flockhart, S. Uppal and R. Pink, Trans. Faraday Soc., 1971, **67**, 513–525.

34 Y. Lan, C. Li, J. Mao and J. Sun, Chemosphere, 2008, **71**, 781–787.